Appl Biochem Biotechnol (2018) 185:863–874
https://doi.org/10.1007/s12010-018-2700-z

Radiolabeled GX1 Peptide for Tumor Angiogenesis Imaging

Érica Aparecida de Oliveira[1,2] · **Bluma Linkowski Faintuch**[1] · **Daniele Seo**[1] · **Angélica Bueno Barbezan**[3] · **Ana Funari**[3] · **Roselaine Campos Targino**[4] · **Ana Maria Moro**[4]

Received: 23 November 2017 / Accepted: 15 January 2018 /
Published online: 24 January 2018

Abstract Early and accurate detection of primary or metastatic tumors is of great value in staging, treatment management, and prognosis. Tumor angiogenesis plays an essential role in the growth, invasion, and metastatic spread of solid cancers, and so, is a promising approach for tumor imaging. The GX1 (CGNSNPKSC) peptide was identified by phage display library and has been investigated as a marker for human cancers. This study aims to evaluate the ^{99m}Tc-HYNIC-PEG$_4$-c (GX1) as a biomarker for tumor imaging. Our results showed that GX1 specifically binds to tumor cells in vitro. SKMEL28 and MDA-MB231 cells achieved total binding peak at 60 min of incubation. For B16F10 and MKN45 cells, the total and specific binding were similar during all time points, while A549 cell line showed rapid cellular total uptake of the tracer at 30 min of incubation. Biodistribution showed low non-specific uptakes and rapid renal excretion. Melanoma tumors showed enhanced GX1 uptake in animal model at 60 min, and it was significantly blocked by cold peptide. The radiotracer showed tumor specificity, especially in melanomas that are highly vascularized tumors. In this sense, it should be considered in future studies, aiming to evaluate degree of angiogenesis, progression, and invasion of tumors.

✉ Érica Aparecida de Oliveira
ericaoliveira@usp.br

[1] Radiopharmacy Center, Institute of Energy and Nuclear Research, Av. Prof. Lineu Prestes, 2242, São Paulo 05508-000, Brazil

[2] Present address: School of Pharmaceutical Sciences, University of Sao Paulo, Av. Prof. Lineu Prestes, 580 Bloco 17, São Paulo, SP 05508-900, Brazil

[3] Radiation Technology Center, Institute of Energy and Nuclear Research, Av. Prof. Lineu Prestes, 2242, São Paulo 05508-000, Brazil

[4] Laboratory of Biopharmacology in Animal Cells, Butantan Institute, Av. Vital Brasil, 1500, Sao Paulo 05503-900, Brazil

Keywords GX1 peptide · Angiogenesis · Technetium-99 m · Tumor · Radiopharmaceuticals

Introduction

Nuclear medicine plays a pivotal role in the management of patients affected by tumors [1–3]. Although positron emitting radionuclides are increasingly used in clinical medicine, ^{99m}Tc remains important for clinical scintigraphic imaging due to its favorable physical properties (t1/2 = 6 h, Eγ = 140 keV), low cost, and widespread availability. In addition, it can also be easily produced by a generator system (^{99}Mo/^{99m}Tc generator) [4, 5]. A recent report shows that ^{99m}Tc represents approximately 80% of the radioactive isotopes used in nuclear medicine around the world [6].

Metastases and recurrence are the major causes of mortality in cancer patients. Early and accurate detection of primary or metastatic tumors is of great value in staging, treatment management, and prognosis in these patients [7]. In this context, tumor angiogenesis plays an essential role in the growth, invasion, and metastatic spread of solid cancers by facilitating the delivery of oxygen, nutrients, and growth factors to tumor cells, providing the rationale that targeting tumor vasculature is a promising approach for tumor imaging [8].

The literature is full of studies about cancer statistics pointing to the most common and deadly tumors. Melanoma is the most aggressive skin cancer and causes over 80% of all deaths in these patients [9]. Lung tumors is the more fatal worldwide, especially in men [10], followed by gastric cancer as the second [11]. Breast cancer is the most common tumor in women, and the metastasis due this tumor is the main cause of death [12].

Small-molecular compounds, such as peptides, can overcome the limitations of long half-life in circulating plasma and the low permeability in solid tumors, owing to the fact that they can rapidly bind in the tumor lesions due to the higher permeability in the target tissue [13–15].

The GX1 (CGNSNPKSC) peptide was identified by phage display library and recently has been investigated as a marker for human cancers [16–18]. In the literature, there are few reports showing GX1-specific binding in gastric, colorectal, and glioma tumor vasculature [16, 19–21]. All these studies indicate that this peptide holds promise both for targeting and antiangiogenic therapy, not only in early tumors but also as a tracer for staging, therapy, and prognosis management. The radiolabeling efficiency of this GX1 sequence with technetium-99 m was already established and published [22]. The radiotracer has high radiochemical purity; it is hydrophilic with preferential renal excretion, an advantageous property for diagnostic radiopharmaceuticals, and also showed excellent in vitro stability under physiological conditions in human serum remaining intact after 4 h. The biodistribution studies showed that most organs and tissues achieved good clearance by 60 min, an advantage in the development of clinically relevant tracers, and this time point was adopted for this study using tumor-bearing models [22]. This study aims to evaluate the GX1 peptide radiolabeled with technetium-99 m as a promising biomarker for different types of tumor imaging in order to provide a new tool for tumor detection in early stages.

Materials and Methods

All of the chemicals used were reagent-grade (Sigma-Aldrich and Merck, Sao Paulo, Brazil). The conjugated peptide HYNIC-PEG_4-c(GX1), purchased from CPC Scientific Inc. (CA, USA), was diluted in water at the concentration of 774.9 μM.

^{99m}Tc, in the form of Na^{99m}TcO4, was eluted from ^{99}Mo/^{99m}Tc generator (Institute of Energetic and Nuclear Research, IPEN/CNEN, São Paulo, Brazil), which was supplied by the Institute of Energy and Nuclear Research/Brazilian Commission of Nuclear Energy (IPEN/CNEN, São Paulo, Brazil) using 0.9% saline. Silica gel strips (ITLC-SG, Agilent Technologies, CA, USA) were used for instant thin-layer chromatography. Reverse-phase high-performance liquid chromatography (RP-HPLC, Agilent Technologies—1260 Infinity, CA, USA) was also performed using a Symmetry C-18 column (5.0 μm, 100 A, 4.6 × 250 mm, Waters, Milford, MA, USA). Radioactivity measurements were conducted using an automated, well-typed c-counter NaI (Tl) crystal (Canberra, Meriden, CT, USA).

Male *nude* mice (18–20 g) were used for the in vivo studies approved by the Animal Welfare Ethical Committee, and the animals were provided by the Animal Facility of IPEN/CNEN in São Paulo, Brazil.

Radiolabeling and Radiochemical Purity

The conjugated peptide HYNIC-PEG$_4$-c(GX1), in salt form, was dissolved in water (1/1 ml). Radiolabeling was performed adding 0.5 ml of Na^{99m}TcO$_4$ (740 MBq) to a sealed reaction vial containing 20 mg of tricine and 5 mg of EDDA (ethylenediamine-*N*,*N*′-diacetic acid) dissolved in 500 μL of 0.1 M of nitrogenated phosphate buffer solution, 10 μl of conjugated peptide solution (μL/mL), and 5 μL of $SnCl_2{\cdot}2H_2O$ solution in 0.1 N HCl (nitrogen-purged). The reaction was induced by heating the mixture to 100 °C for 20 min. Radiochemical evaluation was performed using instant thin-layer chromatography on silica gel strips, and the mobile phase consisted of methylethylketone (MEK) and a solution of 50% acetonitrile (CH_3CN).

Each of the radiolabeled conjugates was also characterized by reverse-phase high-performance liquid chromatography analysis. The HPLC solvents consisted of H_2O, which contained 0.1% trifluoroacetic acid (solvent A), and CH_3CN, which contained 0.1% trifluoroacetic acid (solvent B). The HPLC gradient system began with a solvent composition of 95% A and 5% B, which was followed by a linear gradient of 30% A and 70% B from 0 to 25 min and 5% A and 95% B from 25 to 30 min.

Cell Culture

Tumor cell lines B16F10 (murine melanoma/CRL-6475), SKMEL28 (human melanoma/HTB-72), A549 (human lung adenocarcinoma/CCL-185), MDA-MB231 (human breast adenocarcinoma/HTB-26), and MKN45 (human gastric adenocarcinoma/CRL-1739) obtained from the American Type Culture Collection (ATCC, VA, USA) were cultured in monolayers in DMEM (Dulbecco's modified Eagle's medium) or RPMI medium (Roswell Park Memorial Institute-1640 medium), supplemented with 10% fetal bovine serum, in an humidified atmosphere of 5% CO_2 at 37 °C. After being harvested by centrifuging, cells were resuspended, either in fresh medium containing 0.1% bovine serum albumin (BSA), for in vitro receptor binding assay, or in pH 7.4 phosphate-buffered saline (PBS), for tumor inoculation in animals.

In Vitro Cell Binding Experiments

The cells were seeded in six-well plates (10^6 cells/well) and cultivated for 24 h before the experiments. The culture medium was replaced by fresh medium with only 1% o FCS. ^{99m}Tc-HYNIC-PEG$_4$-c(GX1) (100 μL) was added to the cell culture (5.55 mBq/well), and incubated

for various time periods (from 5 to 120 min) at 37 °C. Unlabeled conjugated peptide (1 μM) was used for blocking evaluation. The supernatant was collected, and cell surface-bound radioligand was removed by acid wash buffer (50 mM glycine buffer pH 2.8, 0.1 M NaCl) at room temperature for 5 min. Internalized radioligand was determined by solubilization of the cells with 1 N NaOH. Results were expressed as percentage of total radioactivity, considering cell surface-bound activity plus internalized activity.

Biodistribution Studies

Experiments were carried out in compliance with the guidelines for animal experimentation, Scientific Ethics Committee, IPEN/CNEN-SP n:88/2011. Suspensions of cells (5×10^6 in 0.1 mL) were subcutaneously injected into the upper back regions of male nude mice. When tumors reached approximately 1 cm diameter, ^{99m}Tc-HYNIC-PEG4-c(GX1) was injected via the tail vein of the mice (50 μl/23 MBq). Gamma-camera images were acquired, whereas samples for biodistribution assessment in different organs and tissues were retrieved, 1 h post injection (p.i.) of the radiotracer. All urethane-anesthetized animals ($n = 5$) were sacrificed by cervical dislocation, and organs and tissues of interest were harvested, weighed, and counted. The radioactivity in each organ was expressed as a percentage of the injected dose per gram of organ (%ID/g).

Receptor blocking studies were also carried out by administration of 100 μg of cold-conjugated peptide diluted in sterile water along with the radiopeptide in the same injection. Using these data, tumor/tissue or tumor/organ ratios were calculated.

Tumor Imaging

Anesthetized mice were horizontally placed under a Mediso Imaging System (Budapest, Hungary), employing a low-energy high-resolution collimator. Images were acquired at 1 h p.i., using a 256 × 256 × 16 matrix size, with a 20% energy window set at 140 keV, for a period of 180 s.

Statistical Analysis

Statistical analyses and graphical representations were generated using GraphPad version 7.0 (GraphPad Software, La Jolla, CA, USA). All data were expressed as mean ± standard deviation (SD). Two-way analysis of variance (ANOVA) was used for comparison and significant differences in the means were determined using multiple comparisons with the Bonferroni test at a significance level of $p < 0.05$.

Results

GX1 Specifically Binds to Tumor Cells In Vitro

Radiochemical purity of ^{99m}Tc-HYNIC-PEG$_4$-c(GX1) was higher than 96% with single peak for each in HPLC analysis, as established in Oliveira and Faintuch [22]. Cell culture studies with tumor cells showed very different binding profiles (Fig. 1). SKMEL28 and MDA-MB231 cells achieved total binding peak at 60 min of incubation, with values of 1.76 ± 0.02% (22% of

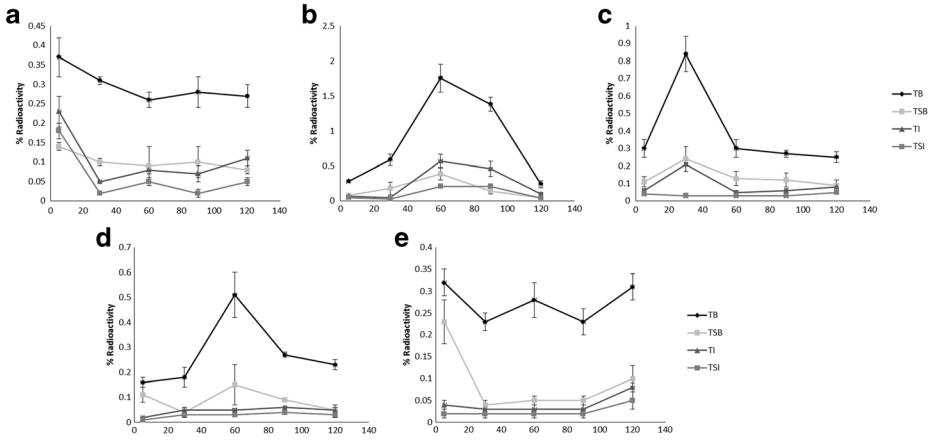

Fig. 1 Uptake binding of ^{99m}Tc-HYNIC-PEG$_4$-c(GX1) in 1 h. **a** B16F10 murine melanoma cells. **b** SKMEL28 human melanoma cells. **c** A549 human lung adenocarcinoma. **d** MDA-MB231 human breast adenocarcinoma. **e** MKN-45 gastric adenocarcinoma. TB total binding, TSB total specific binding, TI total internalization, TSI total specific internalization

specific binding) and 0.51 ± 0.09% (29% of specific binding), respectively. For B16F10 and MKN45 cells, the total and specific binding were similar during all time points, while A549 cell line showed rapid cellular total uptake of the tracer at 30 min of incubation with values of 0.81 ± 0.10%.

Biodistribution of Radiolabeled GX1 Showed Low Non-Specific Uptakes and Rapid Renal Excretion

The results of the biodistribution studies in B16F10, SKMEL28, A549, MDA-MB231, and MKN45 cells at 1 h p.i. are summarized in Table 1. Values are expressed as % of injected dose/g (for blood %ID/mL). The biodistribution revealed predominant renal excretion with a percentage remained in intestinal tract as already reported before by our group. Blood uptake was in the range of 1 to 2% ID/mL and uptake in most organs and tissues around or less than 1% ID/g. The 1-h time adopted for biodistribution and imaging assays were based on blood clearance of the radiotracer in a previous study using *Balb/c* mice [22] and from in vitro results in this work.

Melanoma Tumors Showed Enhanced GX1 Uptake in Animal Model

Biodistribution results showed a remarkable uptake in mice bearing melanoma cells B16F10 and SKMEL28 at 60 min with ^{99m}Tc-HYNIC-PEG$_4$-c(GX1) (1.41 ± 0.18 and 2.42 ± 0.75 %ID/g, respectively). The tumor was 45.39% blocked in B16F10 and 33% in SKMEL28 by GX1 cold peptide, with significant difference when compared to total uptake. The A549, MDA-MB231, and MKN45 cell lines achieved lower uptakes with very similar binding with blocking injection (Fig. 2).

The tumor/muscle ratios in all cell lines are shown in Table 2. The tumor/blood, tumor/bone, and tumor/liver values were higher in animals bearing melanoma tumor cells, reaching 1.05, 2.32, and 2.73 for B16F10 cells, and 1.11, 2.09, and 2.75 for SKMEL28 cells, respectively. Tumor/intestines

Table 1 Biodistribution of ^{99m}Tc-HYNIC-PEG4-c(GX1) in urethane-anesthetized *nude* mice bearing tumor cell lines at 60 min p.i. $n = 5$ and $n = 3$ for block (0.1 mL/18.5 MBq)

	B16F10		SKMEL28		A549		MD MB231		MKN45	
Organ/tissue (%ID/g ± SD)		GX1 Block		GX1 Block		GX1 Block		GX1 Block		GX1 Block
Blood	1.34 ± 1.42	2.84 ± 2.15	2.17 ± 2.03	1.91 ± 0.79	1.57 ± 0.66	1.35 ± 0.64	1.36 ± 0.92	2.06 ± 0.85	0.76 ± 0.62	0.43 ± 0.10
Heart	0.64 ± 0.67	1.02 ± 0.72	0.90 ± 0.68	0.88 ± 0.64	0.44 ± 0.12	0.49 ± 0.17	0.43 ± 0.16	0.63 ± 0.23	0.23 ± 0.15	0.16 ± 0.01
Lungs	1.35 ± 1.27	2.03 ± 1.24	2.16 ± 1.37	1.83 ± 1.20	1.12 ± 0.26	1.39 ± 0.60	1.24 ± 0.41	1.70 ± 0.49	0.82 ± 0.52	0.49 ± 0.07
Kidneys	13.94 ± 1.59	13.83 ± 3.26	14.81 ± 5.34	21.02 ± 13.01	17.35 ± 3.28	12.54 ± 0.97	23.79 ± 3.88	26.73 ± 4.05	16.32 ± 4.52	12.36 ± 0.43
Spleen	0.51 ± 0.41	0.83 ± 0.52	0.94 ± 0.48	0.57 ± 0.20	0.51 ± 0.13	0.79 ± 0.26	0.47 ± 0.05	0.97 ± 0.69	0.34 ± 0.17	0.37 ± 0.21
Stomach	1.49 ± 0.17	1.63 ± 0.86	1.41 ± 0.50	1.04 ± 0.39	3.05 ± 0.79	3.44 ± 1.14	1.32 ± 0.71	1.55 ± 0.44	0.55 ± 0.17	0.58 ± 0.06
Pancreas	0.75 ± 0.73	1.65 ± 1.13	1.47 ± 0.79	1.11 ± 0.86	0.80 ± 0.31	1.29 ± 0.70	0.73 ± 0.25	0.31 ± 0.16	0.43 ± 0.32	0.31 ± 0.16
Liver	0.52 ± 0.25	0.87 ± 0.44	0.88 ± 0.39	0.74 ± 0.45	0.90 ± 0.13	0.90 ± 0.28	0.51 ± 0.30	0.44 ± 0.10	0.33 ± 0.16	0.20 ± 0.04
Large intestine	1.00 ± 0.77	1.47 ± 0.73	1.67 ± 1.14	1.16 ± 0.64	0.78 ± 0.19	1.12 ± 0.51	1.20 ± 0.76	1.04 ± 0.74	0.52 ± 0.24	0.32 ± 0.01
Small intestine	0.60 ± 0.35	1.02 ± 0.47	1.48 ± 0.78	1.24 ± 0.61	0.64 ± 0.29	1.13 ± 0.66	0.91 ± 0.31	0.54 ± 0.31	0.88 ± 0.55	0.33 ± 0.05
Muscle	1.43 ± 1.02	0.71 ± 0.31	0.69 ± 0.21	0.68 ± 0.42	1.15 ± 0.55	3.26 ± 2.49	0.22 ± 0.10	0.30 ± 0.16	0.21 ± 0.06	0.37 ± 0.20
Bone	0.61 ± 0.17	0.72 ± 0.37	1.16 ± 0.56	0.97 ± 0.74	1.14 ± 0.65	1.92 ± 0.91	0.44 ± 0.26	0.69 ± 0.24	1.53 ± 0.89	0.27 ± .18
Brain	0.08 ± 0.04	0.11 ± 0.07	0.14 ± 0.08	0.12 ± 0.10	0.15 ± 0.10	0.08 ± 0.02	0.11 ± 0.11	0.04 ± 0.03	0.05 ± 0.03	0.03 ± 0.02

GX1 Block coinjecting of an excess (50 μL, 1 mg/mL) of unlabeled peptide for receptor blocking

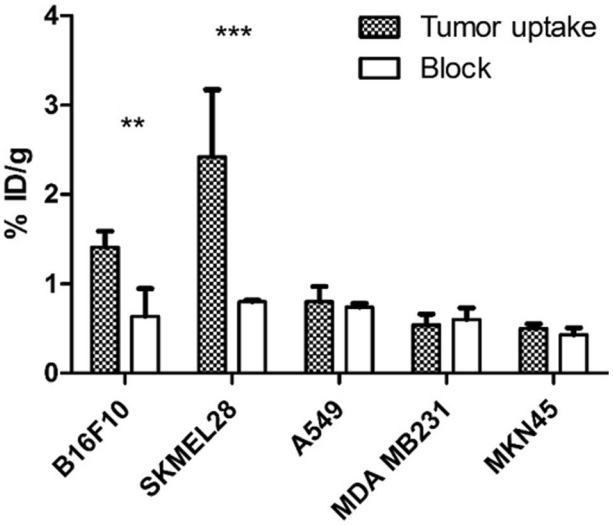

Fig. 2 ^{99m}Tc-HYNIC-PEG$_4$-c(GX1) in vivo uptake. Tumor and blocked tumor of *nude* mice bearing B16F10, SKMEL28, A549, MDA-MB231, and MKN45 1 h after injection. Significances are indicated by $***p < 0.001$ and $**p < 0.01$

and tumor/kidneys were low in all tumors. Tumor/muscle had a range between 0.69 in A549 tumor and 3.51 in SKMEL28 tumor. The images were shown in Fig. 3.

Discussion

The early and specific detection of tumors remains a barrier in oncology. Even though cancer is still one of the leading causes of morbidity and mortality worldwide, with approximately 14 million new cases and 8.2 million deaths per year, as stated by the World Health Organization [23]. Many tumor cells can overexpress surface receptors, due to that small molecule ligands, such as peptides, have been developed to work as biomarkers at earlier stages of malignancy [24–27].

Some features as high stability and integrity under physiological condition and low immunogenicity and toxicity for human trials that would afford massive production are all necessary for clinical translation [27]. For these reasons, this molecule was designed in a cyclic conformation and PEGylation was applied, since it can improve the pharmacokinetic properties [28–30].

Table 2 Tumor/organ and tumor/tissue ratios of ^{99m}Tc-HYNIC-PEG$_4$-c(GX1) 1 h after injection in *nude* mice bearing B16F10, SKMEL28, A549, MDA-MB231, and MKN45 cells

Ratio	B16F10 cells	SKMEL28 cells	A549 cells	MD MB231 cells	MKN45 cells
Tumor/blood	1.05408	1.116189	0.509854	0.395267	0.654934
Tumor/muscle	0.991335	3.517085	0.693607	2.429683	2.383499
Tumor/bone	2.32	2.096317	0.700557	1.216627	0.327735
Tumor/intestines	0.884893	0.770705	0.562364	0.25469	0.586329
Tumor/liver	2.739984	2.752006	0.889804	1.052203	1.49548
Tumor/kidneys	0.10146	0.163582	0.0461	0.022619	0.030672

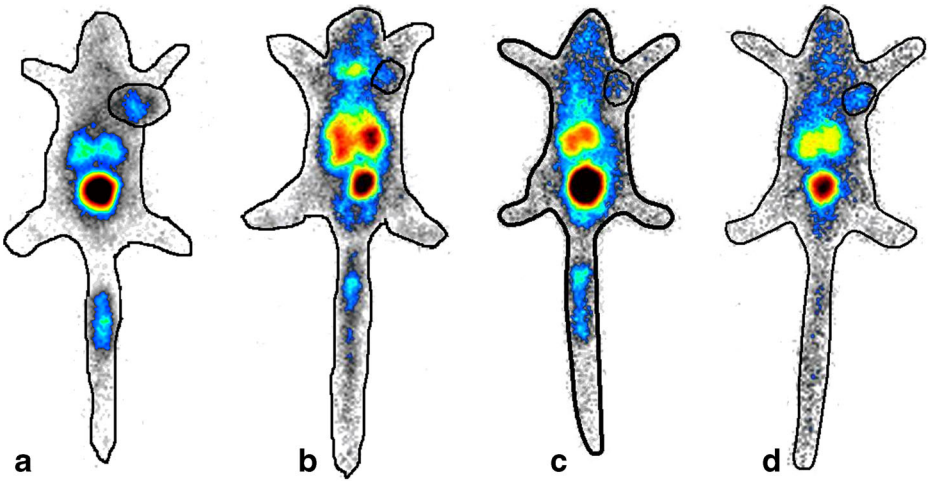

Fig. 3 Scintigraphic image of ^{99m}Tc-HYNIC-PEG$_4$-c(GX1) in xenograft tumor models. Urethane-anesthetized *nude* mice bearing subcutaneous tumor at 1 h p.i. (0.05 mL/18,5 MBq). **a** B16F10 murine melanoma cells. **b** A549 human lung adenocarcinoma. **c** MDA-MB231 human breast adenocarcinoma. **d** MKN-45 gastric adenocarcinoma

A previous study evaluated the same molecule in such aspects, pointing out the high radiochemical purity achieved, the preferential renal excretion, and the optimal blood and organ depuration after 1 h of injection [22]. Based on that, we chose to evaluate the in vivo binding at 1 h p.i., even though the in vitro binding suggested shorter times with higher binding, because without a good body clearance, it is not possible to visualize specific binding in the target tissue.

Nuclear medicine offers a possibility for early cancer diagnosis through molecular imaging modalities such as single-photon emission computed tomography (SPECT) or positron emission tomography (PET) [31, 32]. These techniques are based in premature physiological and biochemical alterations while conventional imaging techniques, such as ultrasonography, X-ray, computerized tomography, and magnetic resonance imaging, detect anatomical and morphological organ changes, which appear only at advanced stages of the disease [33, 34]. Molecular imaging allows less aggressive and multi-targeted treatments of patients leading to better prognostics. Besides that, it would result in a reduction of cancer treatment costs at advanced stages and metastasis [35].

In this context, several peptides have been designed as specific probes for molecular imaging. Many radiolabeled peptides have been introduced into the clinic, for example RGD, bombesin, and somatostatin, with high sensitivity and accuracy for tumor detection [27, 36–40]. Regarding RGD radiotracers, the most recent works indicate the safety and efficiency of these probes radiolabeled, with different radioisotopes, such as ^{99m}Tc and ^{68}Ga, for imaging tumors by SPECT and PET approaches, also including new molecule design, as peptide multiplicity that could increase the binding in the tumor [41–43].

The GX1 peptide has been investigated for glioma imaging with ROI of 5.21 and 1.66% for blocking [19]. Also, Yin et al. [21] in a very similar radiolabeling with ^{99m}Tc and using PEGylation showed in uptake in the range of 1.3% ID/g in LoVo tumors (human colorectal cancer). Du et al. [44] developed a novel theranostic drug platform based in GX1 peptide for fluorescent imaging and therapy of colorectal tumor successfully. GX1 peptides also have been studied for magnetic resonance imaging in orthotopic glioma tumors [45].

We chose to investigate these distinct types of tumors because of their high metastatic potential and due to their relevance in clinical incidence. Melanomas, here represented by B16F10 murine cells and SKMEL28 human cells, are known to be very angiogenic tumors, and for this reason, are expected to present higher uptake of GX1-radiolabeled, as we observed [46, 47]. Although A549 and MDA-MB231 cell lines are frequently used in angiogenesis studies [48, 49], Zhang et al. [50] showed that these cell lines are in a medium level, among several other cell lines, of an important angiogenesis receptor, integrin αvβ3. Also, angiogenic level of gastric cancer is still not clear [51]. These factors can be the reason of the lower uptake of these cells when compared with melanoma models. Following that, xenograft tumors can be well visualized in all situations by gamma-camera imaging, but as expected, the B16F10 melanoma model achieved the best result. Taking all into consideration, this work contributes to the understanding of a target peptide for specific detection of tumors, GX1, which has been investigated as a promising probe for molecular imaging of angiogenic tumors.

Conclusions

The radiotracer showed tumor specificity; however, the performance of ^{99m}Tc-HYNIC-PEG$_4$-c(GX1) in melanomas was better, probably due to difference in the angiogenic level in each tumor analyzed. In this sense, it should be considered in future studies, aiming to evaluate degree of angiogenesis, progression, and invasion of tumors, especially melanoma models.

Acknowledgements The authors are grateful for a postgraduate Grant by Fundação de Amparo a Pesquisa do Estado de São Paulo, Brazil (Fapesp 2011/12405-0). Also, we would like to thank Natanael Gomes da Silva for their technical assistance.

Compliance with Ethical Standards

Conflict of Interest The authors declare that they have no conflict of interest.

References

1. Gorin, M. A., Rowe, S. P., & Denmeade, S. R. (2017). Clinical applications of molecular imaging in the management of prostate cancer. *PET Clin., 12*(2), 185–192. https://doi.org/10.1016/j.cpet.2016.11.001
2. Pennant, M., Takwoingi, Y., Pennant, L., Davenport, C., Fry-Smith, A., Eisinga, A., Andronis, L., Arvanitis, T., Deeks, J., & Hyde, C. (2010). A systematic review of positron emission tomography (PET) and positron emission tomography/computed tomography (PET/CT) for the diagnosis of breast cancer recurrence. *Health Technology Assessment, 14*(50), 1–103. https://doi.org/10.3310/hta14500
3. Niikura, N., Costelloe, C. M., Madewell, J. E., Hayashi, N., Yu, T. K., Liu, J., Palla, S. L., Tokuda, Y., Theriault, R. L., Hortobagyi, G. N., & Ueno, N. T. (2011). FDG-PET/CT compared with conventional imaging in the detection of distant metastases of primary breast cancer. *The Oncologist., 16*(8), 1111–1119. https://doi.org/10.1634/theoncologist.2011-0089
4. Ferro-Flores, G., Ocampo-García, B. E., Santos-Cuevas, C. L., Morales-Avila, E., & Azorín-Vega, E. (2014). Multifunctional radiolabeled nanoparticles for targeted therapy. *Current Medicinal Chemistry, 21*(1), 124–138.
5. Müller, C., & Schibli, R. (2013). Single photon emission computed tomography tracer. *Recent Results in Cancer Research, 187*, 65–105. https://doi.org/10.1007/978-3-642-10853-2_2
6. Dash, A., Knapp, F. F., & Pillai, M. R. A. (2013). 99Mo/99mTc separation: an assessment of technology options. *Nuclear Medicine and Biology, 40*(2), 167–176. https://doi.org/10.1016/j.nucmedbio.2012.10.005
7. Torre, L. A., Siegel, R. L., Ward, E. M., & Jemal, A. (2016). Global cancer incidence and mortality rates and trends—an update. *Cancer Epidemiology, Biomarkers & Prevention, 25*(1), 16–27. https://doi.org/10.1158/1055-9965.EPI-15-0578

8. Folkman, J. (2003). Angiogenesis and apoptosis. *Seminars in Cancer Biology, 13*(2), 159–167. https://doi.org/10.1016/S1044-579X(02)00133-5
9. Ferlay, J., Soerjomataram, I., Dikshit, R., Eser, S., Mathers, C., Rebelo, M., Parkin, D. M., Forman, D., & Bray, F. (2015). Cancer incidence and mortality worldwide: sources, methods and major patterns in GLOBOCAN 2012. *International Journal of Cancer, 136*, E359–E386.
10. American Cancer Society. Key Statistics on Lung Cancer. Available online: www.cancer.org/cancer/non-small-cell-lung-cancer/about/key-statistics.html
11. Hou, Q., Tan, H. T., Lim, K. H., Lim, T. K., Khoo, A., Tan, I. B., Yeoh, K. G., & Chung, M. C. (2013). Identification and functional validation of caldesmon as a potential gastric cancer metastasis-associated protein. *Journal of Proteome Research, 12*(2), 980–990. https://doi.org/10.1021/pr3010259
12. Jemal, A., Bray, F., Center, M. M., Ferlay, J., Ward, E., & Forman, D. (2011). Global cancer statistics. *CA: a Cancer Journal for Clinicians, 61*(2), 69–90. https://doi.org/10.3322/caac.20107
13. Durkan, K., Lambrecht, F. Y., & Unak, P. (2007). Radiolabeling of bombesin-like peptide with 99mTc: 99mTc-litorin and biodistribution in rats. *Bioconjugate Chemistry, 18*(5), 1516–1520. https://doi.org/10.1021/bc060400x
14. Okarvi, S. M. (2004). Peptide-based radiopharmaceuticals: future tools for diagnostic imaging of cancers and other diseases. *Medicinal Research Reviews, 24*(3), 357–397. https://doi.org/10.1002/med.20002
15. Oyen, W. J. G., Bodei, L., Giammarile, F., Maecke, H. R., Tennvall, J., Luster, M., & Brans, B. (2007). Targeted therapy in nuclear medicine—current status and future prospects. *Annals of Oncology, 18*(11), 1782–1792. https://doi.org/10.1093/annonc/mdm111
16. Hu, H., Yin, J., Wang, M., Liang, C., Song, H., Wang, J., Nie, Y., Liang, J., & Wu, K. (2014). GX1 targeting delivery of rmhTNFα evaluated using multimodality imaging. *International Journal of Pharmaceutics, 461*(1–2), 181–191. https://doi.org/10.1016/j.ijpharm.2013.11.016
17. Hui, X., Han, Y., Liang, S., Liu, Z., Liu, J., Hong, L., Zhao, L., He, L., Cao, S., Chen, B., Yan, K., Jin, B., Chai, N., Wang, J., Wu, K., & Fan, D. (2008). Specific targeting of the vasculature of gastric cancer by a new tumor-homing peptide CGNSNPKSC. *Journal of Controlled Release, 131*(2), 86–93. https://doi.org/10.1016/j.jconrel.2008.07.024
18. Zhi, M., Wu, K. C., Dong, L., Hao, Z. M., Deng, T. Z., Hong, L., Liang, S. H., Zhao, P. T., Qiao, T. D., Wang, Y., Xu, X., & Fan, D. M. (2004). Characterization of a specific phage-displayed peptide binding to vasculature of human gastric cancer. *Cancer Biology & Therapy, 3*(12), 1232–1235. https://doi.org/10.4161/cbt.3.12.1223
19. Oliveira, E. A., Faintuch, B. L., Targino, R. C., Moro, A. M., Martinez, R. C., Pagano, R. L., Fonoff, E. T., Carneiro, C. G., Garcez, A. T., Faria, D. P., & Buchpiguel, C. A. (2016). Evaluation of GX1 and RGD-GX1 peptides as new radiotracers for angiogenesis evaluation in experimental glioma models. *Amino Acids, 48*(3), 821–831. https://doi.org/10.1007/s00726-015-2130-y
20. Oliveira, E.A., Lazovic, J., Guo, L., Soto, H., Faintuch, B.L., Akhtari, M., Pope, W. (2017) Evaluation of magnetonanoparticles conjugated with new angiogenesis peptides in intracranial glioma tumors by MRI. Appl Biochem Biotechnol. Mar 9. https://doi.org/10.1007/s12010-017-2443-2.
21. Yin, J., Hui, X., Yao, L., Li, M., Hu, H., Zhang, J., Xin, B., He, M., Wang, J., Nie, Y., & Wu, K. (2015). Evaluation of Tc-99 m labeled dimeric GX1 peptides for imaging of colorectal cancer vasculature. *Molecular Imaging and Biology, 17*(5), 661–670. https://doi.org/10.1007/s11307-015-0838-4
22. Oliveira, E. A., & Faintuch, B. L. (2015). Radiolabeling and biological evaluation of the GX1 and RGD-GX1 peptide sequence for angiogenesis targeting. *Nuclear Medicine and Biology, 42*(2), 123–130. https://doi.org/10.1016/j.nucmedbio.2014.09.004
23. Ferlay, F.B.J., Soerjomataram, I., Ervik, M., Dikshit, R., Eser, S., Mathers, C., Rebelo, M., Parkin, D.M., Forman, D. (2016) GLOBOCAN 2012. Cancer incidence and mortality worldwide: IARC CancerBase No. 11 Int. Agency Res. Cancer, Lyon.
24. Ferreira, C. A., Fuscaldi, L. L., Townsend, D. M., Rubello, D., & Barros, A. L. (2017). Radiolabeled bombesin derivatives for preclinical oncological imaging. *Biomedicine & Pharmacotherapy, 87*, 58–72. https://doi.org/10.1016/j.biopha.2016.12.083
25. Laverman, P., Sosabowski, J. K., Boerman, O. C., & Oyen, W. J. G. (2012). Radiolabelled peptides for oncological diagnosis. *European Journal of Nuclear Medicine and Molecular Imaging, 39*(Suppl. 1), 78–92. https://doi.org/10.1007/s00259-011-2014-7
26. Schottelius, M., & Wester, H. J. (2009). Molecular imaging targeting peptide receptors. *Methods, 48*(2), 161–177. https://doi.org/10.1016/j.ymeth.2009.03.012
27. Sun, X., Li, Y., Liu, T., Li, Z., Zhang, X., Chen, X. (2016) Peptide-based imaging agents for cancer detection. Adv Drug Deliv Ver. S0169-409X(16)30191-0.
28. Adessi, C., & Soto, C. (2002). Converting a peptide into a drug: strategies to improve stability and bioavailability. *Current Medicinal Chemistry, 9*(9), 963–978. https://doi.org/10.2174/0929867024606731

29. Davies, J. S. (2003). The cyclization of peptides and depsipeptides. *Journal of Peptide Science, 9*(8), 471–501. https://doi.org/10.1002/psc.491
30. Hashemi, M., Ayatollahi, S., Parhiz, H., Mokhtarzadeh, A., Javidi, S., & Ramezani, M. (2015). PEGylation of polypropylenimine dendrimer with alkylcarboxylate chain linkage to improve DNA delivery and cytotoxicity. *Applied Biochemistry and Biotechnology, 177*(1), 1–17. https://doi.org/10.1007/s12010-015-1723-y
31. Beer, A. J., Eiber, M., Souvatzoglou, M., Schwaiger, M., & Krause, B. J. (2011). Radionuclide and hybrid imaging of recurrent prostate cancer. *The Lancet Oncology, 12*(2), 181–191. https://doi.org/10.1016/S1470-2045(10)70103-0
32. Higgins, L. J., & Pomper, M. G. (2011). The evolution of imaging in cancer: current state and future challenges. *Seminars in Oncology, 38*(1), 3–15. https://doi.org/10.1053/j.seminoncol.2010.11.010
33. Emonds, K. M., Swinnen, J. V., Mortelmans, L., & Mottaghy, F. M. (2009). Molecular imaging of prostate cancer. *Methods, 48*(2), 193–199. https://doi.org/10.1016/j.ymeth.2009.03.021
34. Santos-Cuevas, C. L., Ferro-Flores, G., Arteaga de Murphy, C., de Ramírez, F. M., Luna-Gutiérrez, M. A., Pedraza-López, M., García-Becerra, R., & Ordaz-Rosado, D. (2009). Design, preparation, in vitro and in vivo evaluation of 99mTc-N2S2-tat(49–57)-bombesin: a target-specific hybrid radiopharmaceutical. *International Journal of Pharmaceutics, 375*(1-2), 75–83. https://doi.org/10.1016/j.ijpharm.2009.04.018
35. Barros, A. L. B., & Fuscaldi, L. L. (2014). Radiolabeled peptides as imaging probes for cancer diagnosis. *J Mol Pharm Org Process Res., 2*, e115.
36. Ambrosini, V., Fani, M., Fanti, S., Forrer, F., & Maecke, H. R. (2011). Radiopeptide imaging and therapy in Europe. *Journal of Nuclear Medicine, 52*(Suppl 2), 42S–55S. https://doi.org/10.2967/jnumed.110.085753
37. Chen, H., Niu, G., Wu, H., & Chen, X. (2016). Clinical application of radiolabeled RGD peptides for PET imaging of integrin αvβ3. *Theranostics., 6*(1), 78–92. https://doi.org/10.7150/thno.13242
38. Mittra, E. S., Goris, M. L., Iagaru, A. H., Kardan, A., Burton, L., Berganos, R., Chang, E., Liu, S., Shen, B., & Chin, F. T. (2011). Pilot pharmacokinetic and dosimetric studies of 18F-FPPRGD2: a PET radiopharmaceutical agent for imaging avb3 integrin levels. *Radiology, 260*(1), 182–191. https://doi.org/10.1148/radiol.11101139
39. Opalinska, M., Hubalewska-Dydejczyk, A., & Sowa-Staszczak, A. (2017). Radiolabeled peptides: current and new perspectives. *The Quarterly Journal of Nuclear Medicine and Molecular Imaging, 61*(2), 153–167. https://doi.org/10.23736/S1824-4785.17.02971-5
40. Christ, E., Wild, D., Forrer, F., Brändle, M., Sahli, R., Clerici, T., Gloor, B., Martius, F., Maecke, H., & Reubi, J. C. (2009). Glucagon-like peptide-1 receptor imaging for localization of insulinomas. *The Journal of Clinical Endocrinology and Metabolism, 94*(11), 4398–4405. https://doi.org/10.1210/jc.2009-1082
41. Kazmierczak, P. M., Todica, A., Gildehaus, F. J., Hirner-Eppeneder, H., Brendel, M., Eschbach, R. S., Hellmann, M., Nikolaou, K., Reiser, M. F., Wester, H. J., Kropf, S., Rominger, A., & Cyran, C. C. (2016). 68Ga-TRAP-(RGD)3 hybrid imaging for the in vivo monitoring of αvß3-integrin expression as biomarker of anti-angiogenic therapy effects in experimental breast cancer. *PLoS One, 11*(12), e0168248. https://doi.org/10.1371/journal.pone.0168248
42. Zhao, Z. Q., Yang, Y., Fang, W., & Liu, S. (2016). Comparison of biological properties of 99mTc-labeled cyclic RGD peptide trimer and dimer useful as SPECT radiotracers for tumor imaging. *Nuclear Medicine and Biology, 43*(11), 661–669. https://doi.org/10.1016/j.nucmedbio.2016.02.006
43. Zhang, J., Niu, G., Lang, L., Li, F., Fan, X., Yan, X., Yao, S., Yan, W., Huo, L., Chen, L., Li, Z., Zhu, Z., & Chen, X. (2017). Clinical translation of a dual integrin αvβ3- and gastrin-releasing peptide receptor-targeting PET radiotracer, 68Ga-BBN-RGD. *Journal of Nuclear Medicine, 58*(2), 228–234. https://doi.org/10.2967/jnumed.116.177048
44. Du, Y., Zhang, Q., Jing, L., Liang, X., Chi, C., Li, Y., Yang, X., Dai, Z., & Tian, J. (2015). GX1-conjugated poly(lactic acid) nanoparticles encapsulating Endostar for improved in vivo anticolorectal cancer treatment. *International Journal of Nanomedicine, 10*, 3791–3802. https://doi.org/10.2147/IJN.S82029
45. Oliveira, E. A., Lazovic, J., Guo, L., Soto, H., Faintuch, B. L., Akhtari, M., & Pope, W. (2017). Evaluation of magnetonanoparticles conjugated with new angiogenesis peptides in intracranial glioma tumors by MRI. *Applied Biochemistry and Biotechnology, 183*(1), 265–279. https://doi.org/10.1007/s12010-017-2443-2
46. Viana, C. T., Campos, P. P., Carvalho, L. A., Cenedezi, J. M., Lavall, L., Lopes, M. T., Ferreira, M. A., & Andrade, S. P. (2013). Distinct types of tumors exhibit differential grade of inflammation and angiogenesis in mice. *Microvascular Research, 86*, 44–51. https://doi.org/10.1016/j.mvr.2012.12.002
47. Oliveira, É. A., Faintuch, B. L., Núñez, E. G., Moro, A. M., Nanda, P. K., & Smith, C. J. (2012). Radiotracers for different angiogenesis receptors in a melanoma model. *Melanoma Research, 22*(1), 45–53. https://doi.org/10.1097/CMR.0b013e32834e6a7e
48. Abdollahi, A., Lipson, K. E., Sckell, A., Zieher, H., Klenke, F., Poerschke, D., Roth, A., Han, X., Krix, M., Bischof, M., Hahnfeldt, P., Grone, H. J., Debus, J., Hlatky, L., & Huber, P. E. (2003). Combined therapy

with direct and indirect angiogenesis inhibition results in enhanced antiangiogenic and antitumor effects. *Cancer Research, 63*(24), 8890–8898.

49. Katkoori, V. R., Basson, M. D., Bond, V. C., Manne, U., & Bumpers, H. L. (2015). Nef-M1, a peptide antagonist of CXCR4, inhibits tumor angiogenesis and epithelial-to-mesenchymal transition in colon and breast cancers. *Oncotarget, 6*(29), 27763–27777. https://doi.org/10.18632/oncotarget.4615
50. Zhang, X., Xiong, Z., Wu, Y., Cai, W., Tseng, J. R., Gambhir, S. S., & Chen, X. (2006). Quantitative PET imaging of tumor integrin alphavbeta3 expression with 18F-FRGD2. *Journal of Nuclear Medicine, 47*(1), 113–121.
51. Aktaş, S. H., Akbulut Yazici, H. O., Zengin, N., Akgün, H. N., Üstüner, Z., & Içli, F. (2017). A new angiogenesis prognostic index with VEGFA, PlGF, and angiopoietin1 predicts survival in patients with advanced gastric cancer. *Turk J Med Sci, 47*(2), 399–406.